Suppressor screen connects HAD protein function to metabolic control in *Plasmodium falciparum*

Ann M. Guggisberg [1]
Aakash Y. Gandhi [1]*
Samuel J. Erlinger [1]#
Emilio F. Merino [2]
Maria B. Cassera [2]
Audrey R. Odom John [1,3]

[1] Department of Pediatrics, Washington University School of Medicine, St. Louis, Missouri, 63110, USA
[2] Department of Biochemistry and Molecular Biology, and Center for Tropical and Emerging Global Diseases (CTEGD), University of Georgia, Athens, GA 30602, USA
[3] Department of Molecular Microbiology, Washington University School of Medicine, St. Louis, Missouri, 63110, USA

Current affiliations:
* Medical Scientist Training Program, University of Texas Southwestern Medical Center, Dallas, Texas, 75235, USA
# Medical Scientist Training Program, Johns Hopkins University, Baltimore, Maryland, 21205, USA

Corresponding author:
Audrey R. Odom John
aodom@wustl.edu

Abstract

In the malaria parasite *Plasmodium falciparum*, isoprenoid synthesis from glycolytic intermediates is essential for survival. The antibiotic and antimalarial fosmidomycin (FSM) inhibits isoprenoid synthesis. In FSM-resistant *P. falciparum*, we identify a loss-of-function mutation in *HAD2* as causative for resistance. Enzymatic characterization shows that HAD2, a member of the haloacid dehalogenase-like hydrolase (HAD) superfamily, functions as a nucleotidase. Harnessing a growth defect in *HAD2*-mutant parasites, we select for suppression of HAD2-mediated FSM resistance and uncover hypomorphic suppressor mutations in the locus encoding the glycolytic enzyme phosphofructokinase. Metabolic profiling demonstrates that

FSM resistance is achieved via increased steady-state levels of MEP pathway and glycolytic intermediates and confirms reduced PFK9 function in the suppressed strains. We identify HAD2 as a novel regulator of malaria glycolytic metabolism and drug sensitivity. Our study informs the biological functions of an evolutionarily conserved family of metabolic regulators and reveal a previously undescribed strategy for cellular glycolytic regulation.

Keywords: Plasmodium, malaria, isoprenoid, resistance, fosmidomycin, suppressor, glycolysis, metabolism, regulation

Introduction

As an obligate intracellular parasite of human erythrocytes, the malaria parasite *Plasmodium falciparum* has unique metabolic features that may be exploited to discover new drug targets and develop new therapies. In the red blood cell niche, *Plasmodium* parasites depend on glucose metabolism. Infection with *Plasmodium* spp. results in a nearly 100-fold increase in glucose import in red blood cells (Mehta, Sonawat, & Sharma, 2006; E. Roth, 1990; E. F. Roth, 1987). Despite these energy requirements, the parasite demonstrates little aerobic respiration via the TCA cycle. Instead, it relies on anaerobic glycolysis to produce ATP (Bowman, Grant, Kermack, & Ogston, 1961; Krungkrai, Burat, Kudan, Krungkrai, & Prapunwattana, 1999; MacRae et al., 2013; Scheibel & Miller, 1969).

Besides ATP production, glucose also has a number of anabolic fates in *P. falciparum*. One such fate is the synthesis of isoprenoids. Isoprenoids are a large class of hydrocarbons with extensive structural and functional diversity (Gershenzon & Dudareva, 2007). In the malaria parasite,

isoprenoids perform several essential functions, including protein prenylation, dolichylation, and synthesis of GPI anchors (Guggisberg, Amthor, & Odom, 2014; Imlay & Odom, 2014; Jordão, Kimura, & Katzin, 2011). Recently, *P. falciparum* isoprenoid intermediates have also been implicated in modulation of vector feeding behavior (Emami et al., 2017).

Despite this diversity, all isoprenoids are synthesized from a common five-carbon building block, isopentyl pyrophosphate (IPP). Evolution has produced two distinct routes for IPP synthesis: the mevalonate pathway, found in archaea, fungi, animals, and the cytoplasm of plants; and the methylerythritol phosphate (MEP) pathway, found in most eubacteria, plant chloroplasts, and apicomplexan parasites such as *P. falciparum* (Lange, Rujan, Martin, & Croteau, 2000). Because of its absence in the human host, the MEP pathway is a compelling target for antimalarial development. The antibiotic and antimalarial fosmidomycin (FSM) is a competitive inhibitor of the first committed enzymatic step of the MEP pathway, catalyzed by 1-deoxy-D-xylulose-5-phosphate reductoisomerase (DXR, E.C. 1.1.1.267) (Koppisch, Fox, Blagg, & Poulter, 2002; Kuzuyama, Shimizu, Takahashi, & Seto, 1998; Steinbacher et al., 2003). FSM has been validated as a specific inhibitor of the MEP pathway in *P. falciparum* (Zhang et al., 2011) and is a valuable chemical tool to study MEP pathway biology and essential metabolism in the parasite.

Parasites are likely to control the proportion of glucose used for energy production versus production of secondary metabolites, such as isoprenoids. We previously used a screen for FSM resistance to identify HAD1, a metabolic regulator whose loss results in increased levels of MEP pathway intermediates and resistance to MEP pathway inhibition. HAD1 is a cytoplasmic sugar phosphatase that can dephosphorylate glycolytic intermediates upstream of the MEP pathway

(Guggisberg, Park, et al., 2014). HAD1 belongs to the haloacid dehalogenase-like hydrolase (HAD) enzyme superfamily (Interpro domain IPR023214) and more specifically, the IIB (IPR006379) and Cof-like hydrolase (IPR000150) subfamilies (Hunter et al., 2012). While HADs are found in all kingdoms of life, HAD1 is most related to bacterial members of this superfamily (Guggisberg, Park, et al., 2014; Kuznetsova et al., 2006), and is implicated in metabolic regulation, stress response, and phosphate homeostasis (M. J. Kang et al., 2005; Y. Kang, Weber, Qiu, Kiley, & Blattner, 2005; Pratish & Radhakrishnan, 2014; Roberts, Lee, McCullagh, Silversmith, & Wemmer, 2005; Sun & Vanderpool, 2013). However, many members of this superfamily remain uncharacterized. The study of HAD proteins in evolutionarily and metabolically distinct organisms such as *P. falciparum* will greatly facilitate our understanding of this ubiquitous class of enzymes.

In this study, we describe the discovery of HAD2, a second HAD family member in *P. falciparum*. We find that HAD2 is required for metabolic homeostasis and normal asexual replication in malaria parasites. Loss of HAD2 dysregulates glycolysis and misroutes metabolites towards the MEP pathway, leading to drug resistance. In vitro, HAD2 dephosphorylates nucleotides. Selection for suppression of drug resistance identifies mutations in *PFK9*, which encodes the canonical glycolytic regulatory enzyme, phosphofructokinase. Through our forward genetics approach, we further define the biological role of the HAD protein superfamily and uncover a novel mechanism of regulation of cellular central carbon metabolism and drug sensitivity.

Results

A nonsense allele of *HAD2*, homolog of the MEP pathway regulator HAD1, in FSM^{R} strain E2

The MEP pathway is responsible for the synthesis of the essential isoprenoid precursors IPP and DMAPP. This pathway is specifically inhibited by the antibiotic fosmidomycin (FSM) (Gisselberg, Dellibovi-Ragheb, Matthews, Bosch, & Prigge, 2013; Yeh & DeRisi, 2011; Zhang et al., 2011). We previously generated *P. falciparum* strains resistant to FSM. Mutations in HAD1 (PF3D7_1033400) cause the resistance phenotype in a majority of these strains (Guggisberg, Park, et al., 2014). However, strain E2 remained uncharacterized. We find that E2 is less sensitive to FSM than its parental line (Figure 1A), as previously reported (Guggisberg, Park, et al., 2014). This resistance phenotype is not due to changes in the *HAD1* locus or changes in *DXS*, *DXR*, or *HAD1* expression (Figure 1-figure supplement 1). To identify genetic changes that may result in FSM resistance, we performed whole genome sequencing (and identified the A469T mutation in PF3D7_1226300 (PlasmoDB ID), hereafter referred to as *HAD2* (Aurrecoechea et al., 2009). Whole genome sequencing data has been deposited in the NCBI BioProject and Sequence Read Archive databases (Guggisberg, Kelly, Hodge, & Odom, 2013a, 2013b). Sanger sequencing of the *HAD2* locus in strain E2 confirmed the presence of the A469T allele. This allele encodes a truncated R157X variant and therefore we expect HAD2 function is lost in strain E2.

Interestingly, HAD2 is a close homolog of the known MEP pathway regulator, the sugar phosphatase HAD1 (Guggisberg, Park, et al., 2014). Sequence homology places both proteins in the haloacid dehalogenase-like hydrolase (HAD) superfamily and further within the IIB and Cof-like hydrolase subfamilies (Interpro IPR006379 and IPR000150, respectively) (Hunter et al., 2012). While no structural information exists for *P. falciparum* HAD2, the structure of the *Plasmodium vivax* HAD2 (PVX_123945, PvHAD2) has been solved (PDB ID 2B30). PvHAD2 (93% identical and 98% similar to PfHAD2) possesses the structural motifs found in other HADs, including a core and cap domain (Figure 1B). HAD2 and HAD1 protein sequences share ~29% sequence identity and ~53% sequence similarity, and HAD2 possesses the four conserved sequence motifs found in HAD proteins (Figure 1C). We hypothesized that HAD2, like HAD1, regulates metabolism in *P. falciparum*.

HAD2 is a nucleotidase

Based on sequence homology to HAD1 and other HAD proteins, we predicted that HAD2 would function enzymatically as a phosphatase. The phosphatase activity of purified recombinant HAD2 was confirmed using *para*-nitrophenyl phosphate (*p*NPP), a chromogenic phospho-substrate (Kuznetsova et al., 2005, 2006) (specific activity, 1.05 ± 0.22 μmol product/min/mg enzyme). Since recent work on the HAD2 homolog from *P. vivax* (PvHAD2) suggested promiscuous substrate recognition, including sugar phosphates and nucleotides (Srinivasan, Kempaiah Nagappa, Shukla, & Balaram, 2015), we determined the substrate specificity of HAD2. Surprisingly, we find markedly weaker activity against sugar phosphate substrates than by HAD1 and its PvHAD2 homolog (Guggisberg, Park, et al., 2014; Srinivasan et al., 2015). In

contrast, we find that HAD2 robustly utilizes several nucleotide substrates (Figure 2). Kinetic parameters for HAD2 against its top five substrates are found in Table 1.

We hypothesized that loss of HAD2-mediated nucleotidase function in FSM^R strain E2 might result in changes in cellular nucleotide levels. We evaluated nucleotide levels using a recently described liquid chromatography-mass spectrometry (LC-MS) method (Laourdakis, Merino, Neilson, & Cassera, 2014). Total steady-state levels of several nucleotides are not altered in strains lacking functional HAD2 (Figure 2-figure supplement 1).

Growth defect of *had2*^{R157X} parasites drives loss of FSM resistance

FSM^R *had2*^{R157X} parasites are growth-attenuated compared to the parental parasite strain (Figure 3, purple vs. black line), a phenotype that is reversed following prolonged culture without FSM. Importantly, we find that improved growth rates also correlate with restored FSM sensitivity. We hypothesized that in FSM^R *had2*^{R157X} parasites, FSM resistance due to loss of HAD2 resulted in a fitness cost. Over time, the FSM^S population would thus predominate. To test this possibility, we selected five clones derived from E2 by limiting dilution in the absence of drug pressure (Figure 4). Three of the five clones were found to be FSM^R (designated clones E2-R1, -R2, and -R3), and two were FSM^S (designated E2-S1 and -S2) (Figure 4). Notably, the FSM^S clones were no longer growth impaired (Figure 3, teal vs. purple line). To our surprise, all five E2 clones had maintained loss of HAD2 via the *had2*^{R157X} mutation.

Long-term culture selects for hypomorphic suppressor mutations in *PFK9*

We hypothesized that these FSM^S E2 clones, driven by a fitness advantage, had acquired new suppressor mutation(s) at an additional locus, resulting in loss of FSM resistance and an increase in growth rate. We performed whole genome sequencing on the five E2 clones to identify any genetic changes that segregated with the FSM^R and FSM^S (suppressed) phenotypes. Indeed, we find that a mutation (*pfk9*^{T1206I}) in the locus encoding phosphofructokinase-9 (*PFK9*, PF3D7_0915400) is present in all the suppressed (FSM^S) E2 clones and none of the FSM^R E2 clones (Figure 4). *PFK9* is the sole mutated genetic locus that segregates with the change in FSM tolerance.

PFK9 encodes phosphofructokinase (PFK, E.C. 2.7.11), which catalyzes the first committed and canonically rate-limiting step of glycolysis, the conversion of fructose 6-phosphate to fructose 1,6-bisphosphate. PFK9 is a single polypeptide, comprised of two domains, alpha and beta (Mony, Mehta, Jarori, & Sharma, 2009) (Figure 5A). While in other eukaryotic systems, the alpha domain is typically regulatory, previous work on *P. falciparum* PFK9 has demonstrated catalytic activity for both domains (Bär, Golbik, Hübner, & Kopperschläger, 2000; Kemp & Gunasekera, 2002; Klinder, Kirchberger, Edelmann, & Kopperschläger, 1998; Mony et al., 2009; Theodorou, Cornel, Duff, & Plaxton, 1992).

We evaluated the effects of the *pfk9*^{T1206I} allele on native PFK activity in *P. falciparum* (Beutler, 1984; Mony et al., 2009) (Figure 5B, Figure 5-figure supplement 1). Lysates from both strains possessing the *pfk9*^{T1206I} mutation (E2-S1, S2) have markedly reduced PFK activity compared to the parental strain (*PFK9*).

Loss of HAD2 leads to dysregulation of glycolysis at PFK9

Since decreased PFK9 activity restored FSM sensitivity to *had2* mutant strains, we postulated that HAD2 normally regulates glycolysis, perhaps at the step catalyzed by PFK9. To evaluate this possibility, we performed targeted metabolic profiling on the parental parasite strain as well as E2 clones R1-R3 and S1-S2 (Figure 5D). Levels of the MEP pathway intermediate DOXP are significantly increased in FSM^R strains lacking HAD2 (Figure 5D, $p \leq 0.05$, one-way ANOVA). As DOXP is the substrate for the FSM target enzyme DXR, our data indicate that FSM^R strain E2 has become FSM resistant because increased levels of DOXP counteract competitive inhibition of DXR by FSM. We also observe increases in the downstream MEP metabolite, MEcPP, in our FSM^R strains.

To understand the role of PFK9 in suppressing FSM resistance, we also determined the steady-state levels of glycolytic intermediates (Figure 5D). We find levels of DOXP and MEcPP are tightly correlated with cellular levels of the PFK9 product, FBP (Pearson $r \geq 0.9$, $p \leq 0.01$). Clustering indicates that resistant clones are characterized by a metabolic signature of increased levels of FBP, DOXP, and MEcPP (Figure 5D). Our results suggest that HAD2 controls metabolic homeostasis at the PFK step. Of note, the *pfk9*^{T1206I} suppressor allele restores nearly parental levels of FBP and downstream MEP pathway intermediates (Figure 5D). Thus, the hypomorphic allele of *PFK9* suppresses the metabolic dysregulation caused by loss of HAD2.

Suppression and complementation support model of HAD2- and PFK9-mediated metabolic regulation

We propose a model of HAD2/PFK9-mediated metabolic regulation (Figure 6). Our data indicate that HAD2 modulates metabolism through nucleotide dephosphorylation and ultimately restricts glycolysis at the level of PFK9. Loss of HAD2 misroutes metabolism, leading to increased substrate availability to the MEP pathway. This results in a substantial fitness cost in asexual growth, which is rescued by reduced PFK9 activity.

In further support of this model, we independently repeated our genetic selection with three FSM^R E2 clones (*had2*^{R157X}, *PFK9*^{WT}), cultured without FSM for >1 month (Figure 4). As before, these strains also lost their FSM resistance phenotype (Figure 4) and restored normal growth (Figure 3). We sequenced *HAD2* and *PFK9* in these three suppressed strains (E2-S3, -S4, and -S5). We find that all strains again maintain the *had2*^{R157X} mutation and acquire new, independent *PFK9* mutations, correlating with increased growth rate and FSM sensitivity (Figures 3 and 4). Of the four PFK9 variants identified in this study, three variants map to the alpha domain, while one variant (S335L) maps to the beta domain (Figure 5A). As with the original T1206I variant found in strains S1 and S2, these additional variants show a significant reduction in PFK activity from lysate (Figure 5B).

Our model also predicted that restoration of functional HAD2 in FSM^R strain E2 should restore FSM sensitivity. Using a piggyback transposon system to express GFP-tagged HAD2 (Balu, Shoue, Fraser, & Adams, 2005; Guggisberg, Park, et al., 2014; Muralidharan, Oksman, Pal, Lindquist, & Goldberg, 2012), we were repeatedly unable to obtain successful transfectants from the FSM^R clones (*had2*^{R157X}, *PFK9*), perhaps due to reduced overall fitness. However, we were able to rescue loss of HAD2 in a suppressed FSM^S E2 clone (*had2*^{R157X}, *pfk9*^{T1206I}) (Figure 5-

figure supplement 2A). Consistent with our model, expression of HAD2-GFP in *had2*^{R157X}, *pfk9*^{T1206I} parasites led to FSM hyper-sensitivity (Figure 5E, Figure 5-figure supplement 2B). The existence of the *pfk9*^{T1206I} allele in the presence of functional HAD2 seems to reduce parasite fitness, as evidenced by reduced growth (Figure 3, grey vs. teal lines).

Using fluorescence microscopy, we observe that HAD2-GFP is localized throughout the cytoplasm in asexual *P. falciparum* trophozoites and schizonts (Figure 5-figure supplement 2C), but excluded from the digestive food vacuole. This is consistent with the lack of a predicted signal sequence for HAD2 using SignalP, PlasmoAP, and PlasMit algorithms (Foth et al., 2003; Petersen, Brunak, von Heijne, & Nielsen, 2011; Zuegge, Ralph, Schmuker, McFadden, & Schneider, 2001). Overall, our localization suggests that HAD2 primarily accesses monophosphorylated nucleotides in the cytosol.

Discussion

Cells must control levels of critical metabolites in order to efficiently utilize carbon sources for energy and biosynthesis of essential molecules. Cells may regulate their metabolism via transcriptional, post-transcriptional, post-translational, allosteric, or enzymatic mechanisms that are necessary for growth (Blume et al., 2015; Brown, Brown, Netea, & Gow, 2014; Jurica et al., 1998; Kronstad et al., 2012). In the glucose-rich red blood cell niche, *Plasmodium* spp. malaria parasites display a unique dependence on glycolysis for energy and biosynthesis.

Using resistance to a metabolic inhibitor, we identify a nucleotidase, HAD2, as a novel regulator of metabolism. Cells lacking HAD2 exhibit marked dysregulation of central carbon metabolism, including altered steady-state levels of glycolytic intermediates and isoprenoid precursors. HAD2 is necessary for optimum parasite fitness, and strains lacking HAD2 acquire additional genetic changes that suppress HAD2-mediated drug resistance and growth defect. We find that mutations in phosphofructokinase (*PFK9*) restore wild-type growth rates and FSM sensitivity. Our study thus directly genetically connect the function of HAD2, a HAD superfamily member, to control of essential central carbon metabolism, as outlined in our model (Figure 6).

In our study, we find that inhibitor resistance is defined by a distinct metabolic signature, characterized by increased levels of the MEP pathway metabolites DOXP and MEcPP and the key glycolytic metabolite FBP. This finding suggests that MEP pathway metabolism is precisely linked to FBP production. In other microbial systems, FBP levels reflect metabolic flux and are cued to environmental perturbations (Kochanowski et al., 2012). FBP-centered metabolic regulation is also important to the related apicomplexan *Toxoplasma gondii*, which constitutively expresses the fructose 1,6-bisphosphatase (FBPase) to fine-tune glucose metabolism (Blume et al., 2015). While *P. falciparum* does not appear to possess an FBPase, necessary for gluconeogenesis, the parasite may possess alternative FBP-sensing mechanisms to tune metabolism, perhaps via regulators such as HAD1 and HAD2.

HAD2 is a member of the HAD superfamily and a homolog of the previously described metabolic regulator HAD1. With our previous studies on HAD1 (Guggisberg, Park, et al., 2014;

Park, Guggisberg, Odom, & Tolia, 2015), we define the role of these proteins in *P. falciparum* and contribute to the greater understanding of the HADs, an evolutionarily conserved and widespread protein family. Both enzymes belong to the IIB (IPR006379) and Cof-like hydrolase (IPR000150) subfamilies (Hunter et al., 2012). HAD enzymes display diverse substrate preferences (Cabello-Díaz et al., 2015; José A Caparrós-Martín, McCarthy-Suárez, & Culiáñez-Macià, 2013; José Antonio Caparrós-Martín, Reiland, Köchert, Cutanda, & Culiáñez-Macià, 2007; Huang et al., 2015; Kuznetsova et al., 2006; Liu et al., 2015; Roberts et al., 2005; Titz et al., 2007), and their biological functions are largely unknown. These subfamilies are comprised of proteins from bacteria and plastid-containing organisms (plants and apicomplexans), most of which notably also employ the MEP pathway, suggesting a common function of HADs. As *P. falciparum* HADs influence easily quantified phenotypes (drug tolerance, growth, metabolite levels), the malaria parasite remains an attractive system to study general HAD biology and function.

Our study uncovers two critical, parasite-specific features of metabolism that are required for *P. falciparum* fitness. First, our data indicate that HAD2 is necessary for efficient asexual replication in *P. falciparum*. As HAD2 lacks close mammalian homologs, targeted therapeutics directed against HAD2 are of great interest. Second, our work highlights the central role of the glycolytic enzyme PFK9. While the parasite tolerates substantial reductions in PFK activity in the $had2^{R157X}$ background, such defects reduce the fitness of parasites rescued with HAD2-GFP. A recent kinetic model of parasite glycolysis confirms that PFK has a high flux-control coefficient, is sensitive to competitive inhibition, and can effectively reduce glycolytic flux (Penkler et al., 2015; van Niekerk, Penkler, du Toit, & Snoep, 2016). We thus propose that PFK9

310 is a leading candidate for strategies to target essential glucose metabolism in malaria. Like
311 HAD2, PFK9 is plant-like and evolutionarily divergent from its mammalian homologs (Mony et
312 al., 2009). These differences may be exploited for PFK inhibitor design.
313
314 Finally, our approach demonstrates the power of forward genetics to uncover novel biology in a
315 clinically relevant, non-model organism. We employ a previously described screen for FSM
316 resistance (Guggisberg, Park, et al., 2014) to uncover a novel resistance locus and employ a
317 second selection for parasite fitness to identify changes that suppress our resistance phenotype.
318 While fitness costs associated with antimalarial resistance are well known [summarized in
319 (Gabryszewski et al., 2016; Hastings & Donnelly, 2005; Rosenthal, 2013)], this study represents,
320 to our knowledge, the first to harness this evolutionary trade-off to identify suppressor mutations
321 in a non-target locus. Fitness assessment of resistance mutations may allow for suppressor
322 screening for other antimalarials or other target pathways to reveal new aspects of biology and
323 drug resistance.
324
325

Materials & Methods

Parasite culture maintenance

Unless otherwise indicated, parasites were maintained in a 2% suspension of human erythrocytes in RPMI medium (Sigma Aldrich, St. Louis, MO) modified with 27 mM $NaHCO_3$, 11 mM glucose, 5 mM HEPES, 0.01 mM thymidine, 1 mM sodium pyruvate, 0.37 mM hypoxanthine, 10 µg/mL gentamycin, and 5 g/L Albumax (Thermo Fisher Scientific, Waltham, MA). Parasites were maintained at 37 °C in 5% O_2/5% CO_2/90% N_2.

Generation of FSM^R strain E2 and clones

FSM^R strain E2 was generated as previously described (Guggisberg, Park, et al., 2014). Briefly, a clone of genome reference strain 3D7 (MRA-102, MR4, ATCC, Manassas, VA) was selected with 3 µM FSM. Clones of strain E2 were isolated by limiting dilution.

Quantification of FSM resistance

Assays were performed in opaque 96-well plates with FSM concentrations ranging from 0.63 nM to 1 mM. Asynchronous cultures were seeded at 0.5-1.0% parasitemia. After 3 days, media was removed and parasitemia was measured by DNA content using Picogreen fluorescence as previously described (Corbett et al., 2004). Cells were stained for 10 min in a solution containing 10 mM Tris HCl, 1 mM EDTA, 2% Triton-X 100, and 0.5% Picogreen reagent (Thermo Fisher Scientific). Fluorescence was measured on a POLARStar Omega spectrophotometer (BMG Labtech, Ortenberg, Germany). Half maximal inhibitory concentration (IC_{50}) values were

calculated using Graphpad Prism software (Graphpad Software, La Jolla, CA). At minimum, all assays were performed in triplicate.

Quantitative PCR

Total RNA was extracted from saponin-lysed parasites using the Ambion Purelink RNA Mini kit (Thermo Fisher Scientific) according to kit instructions. An on-column DNase (Qiagen, Venlo, Netherlands) treatment was performed after the first wash step. To synthesize cDNA, one microgram of total RNA was used in reverse transcriptase reactions using the Quantitect Reverse Transcription kit (Qiagen).

PCR reactions were run using Fast SYBR Green PCR Master Mix (Applied Biosystems, Waltham, MA) and 300 nM each primer. Primers used are listed in Supplementary File 1.

Thermocycling was performed on an Applied Biosystems 7500 Fast RT PCR System with the following parameters: 95 °C for 30 seconds and 40 cycles of 95 °C for 3 seconds, 60 °C for 30 seconds. Controls lacking reverse transcriptase and template both produced no significant signal. Melt curve analysis was used to verify that all primer sets produce single products.

Relative expression levels were calculated using the $\Delta\Delta C_t$ method. ΔC_t represents the C_t value of the reference genes (average of *beta tubulin* and *18s rRNA*) subtracted from the target. $\Delta\Delta C_t$ represents the ΔC_t value of the parental sample subtracted from the sample of interest. Fold changes are calculated as $2^{-\Delta\Delta Ct}$. All assays were performed using technical and biological triplicates.

Antisera generation

Anti-HAD1 antisera has been previously described (MRA-1256, MR4, ATCC, Manassas, VA) (Guggisberg, Park, et al., 2014). Polyclonal anti-HAD2 antisera was raised against 6xHis-HAD2 in rabbits, with Titermax as an adjuvant (Cocalico Biologicals, Reamstown, PA). Antisera specificity was confirmed by immunoblot of *P. falciparum* lysate lacking HAD2.

Immunoblotting

Lysates were separated on a polyacrylamide gel and transferred to a polyvinylidene difluoride membrane. Membranes were blocked in 5% non-fat dry milk, 0.1% Tween-20 in PBS. Rabbit polyclonal antisera were used at the following dilutions: anti-HAD2, 1:2,000-5,000; anti-HAD1 (Guggisberg, Park, et al., 2014), 1:20,000; anti-heat shock protein 70 (Hsp70), 1:5,000 (AS08 371, Agrisera Antibodies, Vännäs, Sweden). All blots used an HRP-conjugated goat anti-rabbit IgG secondary antibody at 1:20,000 (ThermoFisher Scientific 65-6120). When necessary, blots were stripped by washing with 200 mM glycine, 0.1% SDS, 1% Tween-20, pH 2.2 before re-probing.

Whole genome sequencing and SNP analysis

Library preparation, Illumina sequencing, read alignment, and variant analysis were performed by the Washington University Genome Technology Access Center (GTAC, St. Louis, MO). Parasite genomic DNA was prepared for sequencing as previously described (Guggisberg, Park, et al., 2014). One microgram of genomic DNA was sheared, end repaired, and adapter ligated.

Libraries were sequenced on an Illumina HiSeq 2500 in Rapid Run mode to generate 101 bp paired end reads. Reads were aligned to the *P. falciparum* 3D7 reference genome (PlasmoDB v7.2) using Novoalign (V2.08.02). Duplicate reads were removed. SNPs were called using samtools, using a quality score cutoff of 20 and a read depth cutoff of 5. SNPs were annotated using snpEff. Parental SNPs were removed using previously sequenced parental genomes (Guggisberg, Park, et al., 2014). Data has been deposited in the NCBI BioProject database (PRJNA222697) and Sequence Read Archive (SRP038937).

Sanger sequencing

The E2 A469T (R157X) *HAD2* SNP was verified by amplifying *P. falciparum* genomic DNA using primers HAD2_R157X_F and HAD2_R157X_R. The *PFK9* locus was amplified using the PFK9_F and PFK9_R primers. Amplicons were sequenced using the PFK9_seq_(1-8) primers. Primer sequences can be found in Supplementary File 1.

Generation of recombinant protein

The predicted coding sequence of *HAD2* (PlasmoDB ID PF3D7_1226300) was amplified from *P. falciparum* genomic DNA by PCR using the HAD2_LIC_F and HAD2_LIC_R primers (Supplementary File 1). Ligation-independent cloning was used to clone the PCR product into vector BG1861 (Alexandrov et al., 2004), which introduces an N-terminal 6xHis fusion to the expressed protein. BG1861:6xHis-HAD2 construct was transformed into One Shot BL21(DE3)pLysS *Escherichia coli* cells (Thermo Fisher Scientific) according to supplier instructions. Protein expression was induced for 3 hours with isopropyl-β-D-thiogalactoside at mid-log phase (OD_{600} 0.4 – 0.5). Cells were collected by centrifugation and stored at -20°C.

Induced cell pellets were lysed in buffer containing 1 mg/mL lysozyme, 20 mM imidazole, 1 mM dithiothreitol, 10 mM Tris HCl (pH 7.5), 30 U benzonase (EMD Millipore, Darmstadt, Germany), and Complete Mini EDTA-free protease inhibitor tablets (Roche Applied Science, Penzberg, Germany). 6xHis-HAD2 was bound to nickel agarose beads (Gold Biotechnology, Olivette, MO) and eluted in 300 mM imidazole, 20mM Tris HCl (pH 7.5), and 150 mM NaCl. This eluate was further purified by size-exclusion gel chromatography using a HiLoad 16/600 Superdex 200 pg column (GE Healthcare, Chicago, IL) equilibrated in 50 mM Tris HCl (pH 7.5), 1 mM dithiothreitol, and 1 mM $MgCl_2$. The elution fractions containing HAD2 were pooled into a centrifugal filter and concentrated to approximately 3 mg/ml. Glycerol was added to a final concentration of 10% (w/v), and the solution was immediately flash frozen in liquid nitrogen and stored at -80°C. The purification of recombinant HAD1 has been previously described (Guggisberg, Park, et al., 2014).

HAD2 activity assays

Recombinant 6xHis-HAD2 was generated in *E. coli*. HAD2 phosphatase activity was measured against the substrate *p*NPP (New England Biolabs, Ipswich, MA). Phosphatase activity of recombinant enzyme was initially evaluated against the substrate *para*-nitrophenyl phosphate (New England Biolabs). Reactions contained 10 mM *p*NPP, 50 mM Tris HCl (pH 7.5), 5 mM $MgCl_2$, 0.5 mM $MnCl_2$, and 0.25-4 µg enzyme. *Para*-nitrophenyl production was quantified by absorbance at 405 nm. All reactions were performed at 37°C.

Specific enzyme activity against phosphorylated substrates was measured using the EnzChek Phosphate Assay Kit (Thermo Fisher Scientific) according to supplier instructions. Reactions were performed in 50 µL volumes containing 1 mM substrate and 150–750 ng enzyme. Kinetic parameters were determined by continuous measurement of product formation in response to 0.06 – 10 mM substrate. All reactions were performed at 37°C.

Metabolic profiling

All metabolic profiling was performed on ~1 x 10^9 early trophozoites synchronized by treatment with 5% sorbitol. Parasite-infected erythrocytes were lysed with saponin, washed with cold 2 g/L glucose in PBS, and frozen at -80 °C. For measurement of nucleotide levels, samples were extracted and prepared for ultra-high performance liquid chromatography tandem mass spectrometry (IP-RP–UPLC–MS/MS) as previously described (Laourdakis et al., 2014).

For measurement of MEP pathway and glycolytic intermediates, samples were extracted in 600 µL of ice-cold extraction solvent [chloroform, methanol, and acetonitrile (2:1:1, v/v/v)] using two liquid-nitrogen cooled 3.2 mm stainless steel beads and homogenization in a Tissue-Lyser II instrument (Qiagen) at 20 Hz for 5 minutes in a cold sample rack. Ice-cold water was added and samples were homogenized for 5 more minutes at 20 Hz. Samples were centrifuged at 14,000 rcf at 4°C for 5 min. The polar phase was lyophilized and re-dissolved in 100 µL water and analyzed by LC-MS/MS. LC-MS/MS was performed on a 4000QTRAP system (AB Sciex, Framingham, MA) in multiple-reaction monitoring mode using negative ioniziation and 10 mM tributylammonium acetate (pH 5.1-5.5) as the ion pair reagent. The specific parameters used for analysis of MEP pathway metabolites have been previously described (Zhang et al., 2011).

462 Liquid chromatography separation was performed using ion pair reverse-phase chromatography
463 (Luo, Groenke, Takors, Wandrey, & Oldiges, 2007). The referenced method (Luo et al., 2007)
464 was modified: (1) RP-hydro 100 mm × 2.0 mm, 2.5 μm high performance liquid chromatography
465 column (Phenomenex, Torrance, CA), (2) flow rate of 0.14 mL/min, (3) solvent A of 10 mM
466 tributylammonium acetate in 5% methanol, (4) binary LC gradient (20% solvent B (100%
467 methanol) from 0 to 2.5 min, 30% B for 12.5 min, 80% B for 5 min, and column equilibration at
468 for 5 minutes), and (5) 20 μL autosampler injection volume.
469

470 ## *P. falciparum* growth assays

471 Asynchronous cultures were seeded at 1% parasitemia (percent of infected red blood cells).
472 Media was exchanged daily. All assays were performed in the absence of drug pressure. Samples
473 were fixed in 4% paraformaldehyde, 0.05% glutaraldehyde in PBS. Fixed samples were stained
474 with 0.01 mg/ml acridine orange and parasitemia was determined on a BD Biosciences LSRII
475 flow cytometer (Thermo Fisher Scientific). All assays were performed using biological
476 triplicates, at minimum.
477

478 ## Assay of PFK9 activity from lysate

479 Sorbitol-synchronized trophozites were isolated using 0.1% saponin. Cell pellets were washed
480 three times in buffer [100 mM Tris-HCl (pH 7.5), 1 mM $MgCl_2$, 1 mM DTT, 10% glycerol, and
481 EDTA-free protease inhibitor tablets (Roche)]. Lysates were prepared by sonication at 4°C
482 (Fisher Scientific Model 550 Sonic Dismembrator, amplitude 3.5), followed by centrifugation at
483 4°C (10,000 x *g*, 10 min).
484

PFK9 activity in lysate was monitored by linking it to the oxidation of NADH, as described previously (Beutler, 1984; Mony et al., 2009). Reactions contained 100 mM Tris-HCl (pH 7.5), 1 mM $MgCl_2$, 1 mM DTT, 0.25 mM NADH, 1 mM ATP, 3 mM fructose 6-phosphate, as well as excess of linking enzymes aldolase (7.5 U), triose-phosphate isomerase (3.8 U), and glycerol 3-phosphate dehydrogenase (3.8 U). After adding fresh cell lysate (15 µg total protein), the absorbance at 340 nm was measured at 37°C for 40 min. Activity (µmol/min/mg total protein) was determined by linear regression using Graphpad Prism software. All assays were performed using technical and biological triplicates.

pTEOE110:HAD2 plasmid construction

The pTEOE110:HAD2-GFP construct contains the *heat shock protein 110* (PF3D7_0708800) 5' UTR and a C-terminal GFP tag. Human dihydrofolate reductase (hDHFR) is present as a selectable marker. Inverted terminal repeats are included for integration into the genome by a co-transfected piggyBac transposase (pHTH, MRA912, MR4, ATCC, Manassas, VA).

HAD2 was amplified with the HAD2_XhoI_F and HAD2_AvrII_R primers (Supplementary File 1) and cloned into AvrII and XhoI sites in the pTEOE110 plasmid.

Parasite transfections

Transfections were performed as previously described (Guggisberg, Park, et al., 2014). Briefly, 50-100 µg of plasmid DNA was precipitated and resuspended in Cytomix (25 mM HEPES pH 7.6, 120 mM KCl, 0.15 mM $CaCl_2$, 2mM EGTA, 5 mM $MgCl_2$, 10 mM K_2HPO_4).

A ring-stage *P. falciparum* culture was washed with Cytomix and resuspended in the DNA/Cytomix solution. The culture was electroporated at 950 µF and 0.31 kV, washed with media, and returned to normal culture conditions. Parasites expressing the construct were selected by continuous treatment with 5 nM WR92210 (Jacobus Pharmaceuticals, Princeton, NJ). Transfectants were cloned by limiting dilution and presence of the HAD2-GFP construct was verified by PCR using gene-specific and GFP-specific primers (HAD2_R157X_F and GFP_R, Supplementary File 1). The presence of the endogenous $had2^{R157X}$ and $pfk9^{T1206I}$ mutations were verified by Sanger sequencing.

Live fluorescent microscopy

Erythrocytes infected with E2 Hsp110:HAD2-GFP parasites were stained with 10 ng/µL Hoescht 33258 and mounted under coverslips on polysine adhesion slides. Cells were viewed on an Olympus BH8 microscope (Tokyo, Japan). Minimal adjustments to contrast and brightness were applied equally to all microscopy images using Inkscape.

Author contributions

Conceptualization, A.M.G., A.Y.G., and A.R.O.J.; Investigation, A.M.G., A.Y.G., E.F.M., and M.B.C.; Resources, A.M.G. and S.J.E.; Writing – Original Draft, A.M.G. and A.R.O.J.; Writing – Review and Editing, A.M.G., A.Y.G., S.J.E., E.F.M, M.B.C, and A.R.O.J; Visualization, A.M.G. and A.Y.G.; Supervision, A.R.O.J.; Funding acquisition, A.R.O.J.

Acknowledgments

This work is supported by the NIH/NIAID (R01AI103280 to A.R.O.J. and AI108819 to M.B.C.), the Children's Discovery Institute of Washington University and St. Louis Children's Hospital (MD-LI-2011-171 to A.R.O.J.), the March of Dimes Foundation (Basil O'Connor Starter Scholar Research Award to A.R.O.J.), the Doris Duke Foundation (Clinical Scientist Development Award to A.R.O.J.), the NIH/NIGMS (training grant T32GM007067 to A.M.G.), the Monsanto Excellence Fund at Washington University (graduate fellowship to A.M.G.), a HHMI Summer Undergraduate Research Fellowship (to A.Y.G.), and an ASM Undergraduate Research Fellowship (to A.Y.G.). We thank the Proteomics and Mass Spectrometry Facility at the Donald Danforth Plant Science Center for assistance with LC-MS/MS. This work was supported by the National Science Foundation under grant number DBI-0521250 for acquisition of the QTRAP LC-MS/MS. We thank Daniel Goldberg (Washington University) for supplying the pTEOE110 plasmid. We thank the Malaria Research Reference and Reagent Resource (MR4) for providing reagents contributed by D.J. Carucci (MRA-102) and John Adams (MRA-912).

References

Alexandrov, A., Vignali, M., LaCount, D. J., Quartley, E., de Vries, C., De Rosa, D., … Grayhack, E. J. (2004). A facile method for high-throughput co-expression of protein pairs. *Molecular & Cellular Proteomics*, *3*(9), 934–8.

Aurrecoechea, C., Brestelli, J., Brunk, B. P., Dommer, J., Fischer, S., Gajria, B., … Wang, H. (2009). PlasmoDB: a functional genomic database for malaria parasites. *Nucleic Acids Research*, *37*(Database issue), D539-43.

Balu, B., Shoue, D. A., Fraser, M. J., & Adams, J. H. (2005). High-efficiency transformation of *Plasmodium falciparum* by the lepidopteran transposable element piggyBac. *Proceedings of the National Academy of Sciences of the United States of America*, *102*(45), 16391–6.

Bär, J., Golbik, R., Hübner, G., & Kopperschläger, G. (2000). Denaturation of phosphofructokinase-1 from *Saccharomyces cerevisiae* by guanidinium chloride and reconstitution of the unfolded subunits to their catalytically active form. *Biochemistry*, *39*(23), 6960–8.

Beutler, E. (1984). *Red Cell Metabolism: A Manual of Biochemical Methods*. Philadelphia, PA: Grune & Stratton.

Blume, M., Nitzsche, R., Sternberg, U., Gerlic, M., Masters, S. L., Gupta, N., & McConville, M. J. (2015). A *Toxoplasma gondii* gluconeogenic enzyme contributes to robust central carbon metabolism and is essential for replication and virulence. *Cell Host & Microbe*, *18*(2), 210–20.

Bowman, I. B., Grant, P. T., Kermack, W. O., & Ogston, D. (1961). The metabolism of *Plasmodium berghei*, the malaria parasite of rodents. 2. An effect of mepacrine on the metabolism of glucose by the parasite separated from its host cell. *The Biochemical Journal*, *78*(3), 472–8.

Brown, A. J. P., Brown, G. D., Netea, M. G., & Gow, N. A. R. (2014). Metabolism impacts upon Candida immunogenicity and pathogenicity at multiple levels. *Trends in Microbiology*, *22*(11), 614–622.

Burroughs, A. M., Allen, K. N., Dunaway-Mariano, D., & Aravind, L. (2006). Evolutionary genomics of the HAD superfamily: understanding the structural adaptations and catalytic diversity in a superfamily of phosphoesterases and allied enzymes. *Journal of Molecular Biology*, *361*(5), 1003–34.

Cabello-Díaz, J. M., Gálvez-Valdivieso, G., Caballo, C., Lambert, R., Quiles, F. A., Pineda, M., & Piedras, P. (2015). Identification and characterization of a gene encoding for a nucleotidase from *Phaseolus vulgaris*. *Journal of Plant Physiology*, *185*, 44–51.

Caparrós-Martín, J. A., McCarthy-Suárez, I., & Culiáñez-Macià, F. A. (2013). HAD hydrolase function unveiled by substrate screening: enzymatic characterization of *Arabidopsis thaliana* subclass I phosphosugar phosphatase AtSgpp. *Planta*, *237*(4), 943–54.

Caparrós-Martín, J. A., Reiland, S., Köchert, K., Cutanda, M. C., & Culiáñez-Macià, F. A. (2007). *Arabidopsis thaliana* AtGppl and AtGpp2: two novel low molecular weight phosphatases involved in plant glycerol metabolism. *Plant Molecular Biology*, *63*(4), 505–17.

Corbett, Y., Herrera, L., Gonzalez, J., Cubilla, L., Capson, T. L., Coley, P. D., … Ortega-Barria, E. (2004). A novel DNA-based microfluorimetric method to evaluate antimalarial drug activity. *American Journal of Tropical Medicine and Hygiene*, *70*(2), 119–24.

Emami, S. N., Lindberg, B. G., Hua, S., Hill, S., Mozuraitis, R., Lehmann, P., … Faye, I. (2017).

590 A key malaria metabolite modulates vector blood seeking, feeding, and susceptibility to
591 infection. *Science*, *355*(6329), 1076–1080.
592 Foth, B. J., Ralph, S. A., Tonkin, C. J., Struck, N. S., Fraunholz, M., Roos, D. S., … McFadden,
593 G. I. (2003). Dissecting apicoplast targeting in the malaria parasite *Plasmodium falciparum*.
594 *Science*, *299*(5607), 705–8.
595 Gabryszewski, S. J., Dhingra, S. K., Combrinck, J. M., Lewis, I. A., Callaghan, P. S., Hassett, M.
596 R., … Fidock, D. A. (2016). Evolution of fitness cost-neutral mutant PfCRT conferring *P.*
597 *falciparum* 4-aminoquinoline drug resistance is accompanied by altered parasite metabolism
598 and digestive vacuole physiology. *PLOS Pathogens*, *12*(11), e1005976.
599 Gershenzon, J., & Dudareva, N. (2007). The function of terpene natural products in the natural
600 world. *Nature Chemical Biology*, *3*(7), 408–14.
601 Gisselberg, J. E., Dellibovi-Ragheb, T. A., Matthews, K. A., Bosch, G., & Prigge, S. T. (2013).
602 The Suf iron-sulfur cluster synthesis pathway is required for apicoplast maintenance in
603 malaria parasites. *PLoS Pathogens*, *9*(9), e1003655.
604 Guggisberg, A. M., Amthor, R. E., & Odom, A. R. (2014). Isoprenoid biosynthesis in
605 Plasmodium falciparum. *Eukaryotic Cell*, *13*(11), 1348–59.
606 Guggisberg, A. M., Kelly, M. L., Hodge, D. M., & Odom, A. R. (2013a). Fosmidomycin-
607 resistant *Plasmodium falciparum* whole genome sequencing. *NCBI BioProject Database*,
608 (PRJNA222697).
609 Guggisberg, A. M., Kelly, M. L., Hodge, D. M., & Odom, A. R. (2013b). Fosmidomycin-
610 resistant *Plasmodium falciparum* whole genome sequencing. *Sequence Read Archive*,
611 (SRP038937).
612 Guggisberg, A. M., Park, J., Edwards, R. L., Kelly, M. L., Hodge, D. M., Tolia, N. H., & Odom,
613 A. R. (2014). A sugar phosphatase regulates the methylerythritol phosphate (MEP) pathway
614 in malaria parasites. *Nature Communications*, *5*, 4467.
615 Hastings, I. M., & Donnelly, M. J. (2005). The impact of antimalarial drug resistance mutations
616 on parasite fitness, and its implications for the evolution of resistance. *Drug Resistance*
617 *Updates*, *8*(1), 43–50.
618 Huang, H., Pandya, C., Liu, C., Al-Obaidi, N. F., Wang, M., Zheng, L., … Farelli, J. D. (2015).
619 Panoramic view of a superfamily of phosphatases through substrate profiling. *Proceedings*
620 *of the National Academy of Sciences of the United States of America*, *112*(16), E1974-83.
621 Retrieved from http://www.ncbi.nlm.nih.gov/pubmed/25848029
622 Hunter, S., Jones, P., Mitchell, A., Apweiler, R., Attwood, T. K., Bateman, A., … Yong, S.-Y.
623 (2012). InterPro in 2011: new developments in the family and domain prediction database.
624 *Nucleic Acids Research*, *40*(Database issue), D306-12.
625 Imlay, L., & Odom, A. R. (2014). Isoprenoid metabolism in apicomplexan parasites. *Current*
626 *Clinical Microbiology Reports*, *1*(3–4), 37–50. http://doi.org/10.1007/s40588-014-0006-7
627 Jordão, F. M., Kimura, E. A., & Katzin, A. M. (2011). Isoprenoid biosynthesis in the
628 erythrocytic stages of Plasmodium falciparum. *Memórias Do Instituto Oswaldo Cruz*, *106*,
629 134–141.
630 Jurica, M. S., Mesecar, A., Heath, P. J., Shi, W., Nowak, T., & Stoddard, B. L. (1998). The
631 allosteric regulation of pyruvate kinase by fructose-1,6-bisphosphate. *Structure*, *6*(2), 195–
632 210.
633 Kang, M. J., Lee, Y. M., Yoon, S. H., Kim, J. H., Ock, S. W., Jung, K. H., … Kim, S. W. (2005).
634 Identification of genes affecting lycopene accumulation in *Escherichia coli* using a shot-gun
635 method. *Biotechnology and Bioengineering*, *91*(5), 636–42.

636 Kang, Y., Weber, K. D., Qiu, Y., Kiley, P. J., & Blattner, F. R. (2005). Genome-wide expression
637 analysis indicates that FNR of *Escherichia coli* K-12 regulates a large number of genes of
638 unknown function. *Journal of Bacteriology*, *187*(3), 1135–1160.
639 Kemp, R. G., & Gunasekera, D. (2002). Evolution of the allosteric ligand sites of mammalian
640 phosphofructo-1-kinase. *Biochemistry*, *41*(30), 9426–30.
641 Klinder, A., Kirchberger, J., Edelmann, A., & Kopperschläger, G. (1998). Assembly of
642 phosphofructokinase-1 from *Saccharomyces cerevisiae* in extracts of single-deletion
643 mutants. *Yeast*, *14*(4), 323–34.
644 Kochanowski, K., Volkmer, B., Gerosa, L., Haverkorn van Rijsewijk, B. R., Schmidt, A., &
645 Heinemann, M. (2012). Functioning of a metabolic flux sensor in *Escherichia coli*.
646 *Proceedings of the National Academy of Sciences*, *110*(3), 1130–1135.
647 Koppisch, A. T., Fox, D. T., Blagg, B. S. J., & Poulter, C. D. (2002). *E. coli* MEP synthase:
648 steady-state kinetic analysis and substrate binding. *Biochemistry*, *41*(1), 236–43.
649 Kronstad, J., Saikia, S., Nielson, E. D., Kretschmer, M., Jung, W., Hu, G., … Attarian, R. (2012).
650 Adaptation of *Cryptococcus neoformans* to mammalian hosts: integrated regulation of
651 metabolism and virulence. *Eukaryotic Cell*, *11*(2), 109–18.
652 Krungkrai, J., Burat, D., Kudan, S., Krungkrai, S., & Prapunwattana, P. (1999). Mitochondrial
653 oxygen consumption in asexual and sexual blood stages of the human malarial parasite,
654 *Plasmodium falciparum*. *The Southeast Asian Journal of Tropical Medicine and Public*
655 *Health*, *30*(4), 636–42.
656 Kuznetsova, E., Proudfoot, M., Gonzalez, C. F., Brown, G., Omelchenko, M. V, Borozan, I., …
657 Yakunin, A. F. (2006). Genome-wide analysis of substrate specificities of the *Escherichia*
658 *coli* haloacid dehalogenase-like phosphatase family. *The Journal of Biological Chemistry*,
659 *281*(47), 36149–61.
660 Kuznetsova, E., Proudfoot, M., Sanders, S. A., Reinking, J., Savchenko, A., Arrowsmith, C. H.,
661 … Yakunin, A. F. (2005). Enzyme genomics: Application of general enzymatic screens to
662 discover new enzymes. *FEMS Microbiology Reviews*, *29*(2), 263–79.
663 Kuzuyama, T., Shimizu, T., Takahashi, S., & Seto, H. (1998). Fosmidomycin, a specific inhibitor
664 of 1-deoxy-d-xylulose 5-phosphate reductoisomerase in the nonmevalonate pathway for
665 terpenoid biosynthesis. *Tetrahedron Letters*, *39*(43), 7913–6.
666 Lange, B. M., Rujan, T., Martin, W., & Croteau, R. (2000). Isoprenoid biosynthesis: the
667 evolution of two ancient and distinct pathways across genomes. *Proceedings of the National*
668 *Academy of Sciences of the United States of America*, *97*(24), 13172–7.
669 Laourdakis, C. D., Merino, E. F., Neilson, A. P., & Cassera, M. B. (2014). Comprehensive
670 quantitative analysis of purines and pyrimidines in the human malaria parasite using ion-
671 pairing ultra-performance liquid chromatography-mass spectrometry. *Journal of*
672 *Chromatography. B, Analytical Technologies in the Biomedical and Life Sciences*, *967*,
673 127–33.
674 Liu, J., Zhou, W., Liu, G., Yang, C., Sun, Y., Wu, W., … Cheng, Y. (2015). The conserved
675 endoribonuclease YbeY is required for chloroplast ribosomal RNA processing in
676 Arabidopsis. *Plant Physiology*, *168*(1), 205–221.
677 Luo, B., Groenke, K., Takors, R., Wandrey, C., & Oldiges, M. (2007). Simultaneous
678 determination of multiple intracellular metabolites in glycolysis, pentose phosphate pathway
679 and tricarboxylic acid cycle by liquid chromatography-mass spectrometry. *Journal of*
680 *Chromatography*, *1147*(2), 153–64.
681 MacRae, J. I., Dixon, M. W., Dearnley, M. K., Chua, H. H., Chambers, J. M., Kenny, S., …

McConville, M. J. (2013). Mitochondrial metabolism of sexual and asexual blood stages of the malaria parasite *Plasmodium falciparum*. *BMC Biology*, *11*(1), 67.

Mehta, M., Sonawat, H. M., & Sharma, S. (2006). Glycolysis in *Plasmodium falciparum* results in modulation of host enzyme activities. *Journal of Vector Borne Diseases*, *43*(3), 95–103.

Mony, B. M., Mehta, M., Jarori, G. K., & Sharma, S. (2009). Plant-like phosphofructokinase from *Plasmodium falciparum* belongs to a novel class of ATP-dependent enzymes. *International Journal for Parasitology*, *39*(13), 1441–53.

Muralidharan, V., Oksman, A., Pal, P., Lindquist, S., & Goldberg, D. E. (2012). *Plasmodium falciparum* heat shock protein 110 stabilizes the asparagine repeat-rich parasite proteome during malarial fevers. *Nature Communications*, *3*, 1310.

Park, J., Guggisberg, A. M., Odom, A. R., & Tolia, N. H. (2015). Cap-domain closure enables diverse substrate recognition by the C2-type haloacid dehalogenase-like sugar phosphatase *Plasmodium falciparum* HAD1. *Acta Crystallographica. Section D, Biological Crystallography*, *71*(Pt 9), 1824–34.

Penkler, G., du Toit, F., Adams, W., Rautenbach, M., Palm, D. C., van Niekerk, D. D., & Snoep, J. L. (2015). Construction and validation of a detailed kinetic model of glycolysis in *Plasmodium falciparum*. *The FEBS Journal*.

Petersen, T. N., Brunak, S., von Heijne, G., & Nielsen, H. (2011). SignalP 4.0: discriminating signal peptides from transmembrane regions. *Nature Methods*, *8*(10), 785–6.

Pratish, G., & Radhakrishnan, M. (2014). Engineering *Escherichia coli* for D-ribose production from glucose-xylose mixtures. *Industrial Biotechnology*, *10*(2), 106–114.

Roberts, A., Lee, S.-Y., McCullagh, E., Silversmith, R. E., & Wemmer, D. E. (2005). YbiV from *Escherichia coli* K12 is a HAD phosphatase. *Proteins*, *58*(4), 790–801.

Rosenthal, P. J. (2013). The interplay between drug resistance and fitness in malaria parasites. *Molecular Microbiology*, *89*(6), 1025–1038.

Roth, E. (1990). *Plasmodium falciparum* carbohydrate metabolism: a connection between host cell and parasite. *Blood Cells*, *16*(2–3), 453–66.

Roth, E. F. (1987). Malarial parasite hexokinase and hexokinase-dependent glutathione reduction in the *Plasmodium falciparum*-infected human erythrocyte. *The Journal of Biological Chemistry*, *262*(32), 15678–82.

Scheibel, L. W., & Miller, J. (1969). Glycolytic and cytochrome oxidase activity in Plasmodia. *Military Medicine*, *134*(10), 1074–80.

Srinivasan, B., Kempaiah Nagappa, L., Shukla, A., & Balaram, H. (2015). Prediction of substrate specificity and preliminary kinetic characterization of the hypothetical protein PVX_123945 from *Plasmodium vivax*. *Experimental Parasitology*, *151*, 56–63.

Steinbacher, S., Kaiser, J., Eisenreich, W., Huber, R., Bacher, A., & Rohdich, F. (2003). Structural basis of fosmidomycin action revealed by the complex with 2-C-methyl-D-erythritol 4-phosphate synthase (IspC). Implications for the catalytic mechanism and anti-malaria drug development. *The Journal of Biological Chemistry*, *278*(20), 18401–7.

Sun, Y., & Vanderpool, C. K. (2013). Physiological consequences of multiple-target regulation by the small RNA SgrS in *Escherichia coli*. *Journal of Bacteriology*, *195*(21), 4804–15.

Theodorou, M. E., Cornel, F. A., Duff, S. M., & Plaxton, W. C. (1992). Phosphate starvation-inducible synthesis of the alpha-subunit of the pyrophosphate-dependent phosphofructokinase in black mustard suspension cells. *The Journal of Biological Chemistry*, *267*(30), 21901–5.

Titz, B., Häuser, R., Engelbrecher, A., Uetz, P., Alatossava, T., Jutte, H., … Inouye, M. (2007).

728 The *Escherichia coli* protein YjjG is a house-cleaning nucleotidase in vivo. *FEMS*
729 *Microbiology Letters*, *270*(1), 49–57.
730 van Niekerk, D. D., Penkler, G. P., du Toit, F., & Snoep, J. L. (2016). Targeting glycolysis in the
731 malaria parasite *Plasmodium falciparum*. *The FEBS Journal*, *283*(4), 634–46.
732 Yeh, E., & DeRisi, J. L. (2011). Chemical rescue of malaria parasites lacking an apicoplast
733 defines organelle function in blood-stage *Plasmodium falciparum*. *PLoS Biology*, *9*(8),
734 e1001138.
735 Zhang, B., Watts, K. M., Hodge, D., Kemp, L. M., Hunstad, D. A., Hicks, L. M., & Odom, A. R.
736 (2011). A second target of the antimalarial and antibacterial agent fosmidomycin revealed
737 by cellular metabolic profiling. *Biochemistry*, *50*(17), 3570–7.
738 Zuegge, J., Ralph, S., Schmuker, M., McFadden, G. I., & Schneider, G. (2001). Deciphering
739 apicoplast targeting signals--feature extraction from nuclear-encoded precursors of
740 *Plasmodium falciparum* apicoplast proteins. *Gene*, *280*(1–2), 19–26.
741
742

Figures and Tables

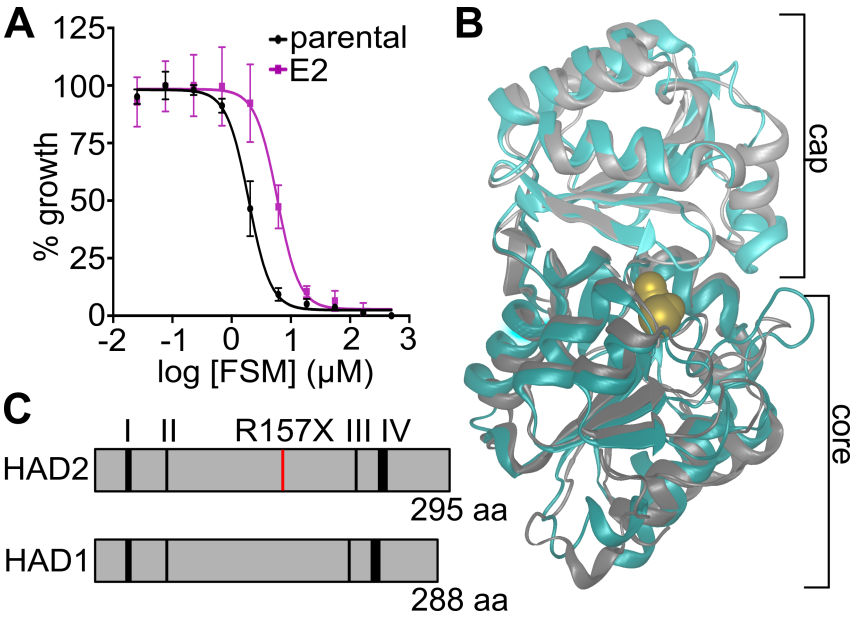

Figure 1. FSM^{R} strain E2 possesses a mutation in HAD2, a homolog of the MEP pathway regulator HAD1. (A) Representative FSM dose-response of the parental strain and strain E2. Strain E2 has a mean IC_{50} of 4.8 ± 1.2 μM (n=7), greater than the parent strain (0.8 ± 0.1 μM), $p \leq 0.01$, unpaired Student's t-test. (**B**) *P. vivax* HAD2 (teal, PDB 2B30) is structurally similar to PfHAD1 (grey, PDB 4QJB). Ions (Mg^{2+}, Ca^{2+}, Cl^{-}) are shown in yellow. (**C**) HAD2 is a homolog of HAD1 (~29% identity and ~53% similarity) and possesses all HAD conserved sequence motifs required for catalysis (Burroughs, Allen, Dunaway-Mariano, & Aravind, 2006).

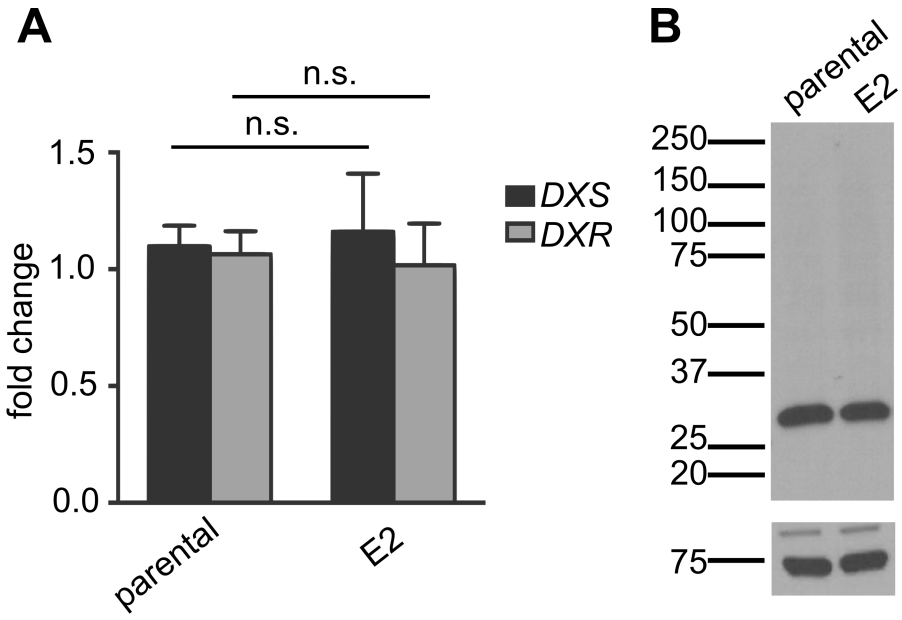

Figure 1-figure supplement 1. FSM^R strain E2 does not have increased expression of *DXS*, *DXR*, or HAD1.

(**A**) *DXS* and *DXR* transcript levels are unchanged in FSM^R strain E2. Shown are mean relative mRNA expression levels determined by qPCR. Error bars represent S.E.M. from duplicate biological replicates, measured using three technical replicates (N.s. = not significant, $p>0.05$, unpaired Student's t-test). (**B**) HAD1 expression is unchanged in FSM^R strain E2. Shown are immunoblots of the parent strain and FSM^R strain E2. Marker units are kilodaltons (kDa). Top panel was probed with anti-HAD1 antisera. Bottom panel was probed with anti-heat shock protein 70 antisera as a loading control. Expected protein masses: HAD1, 33 kDa; Hsp70, 74 kDa. Blot is representative of three independent experiments. Minimal brightness adjustments were applied equally to all blot images.

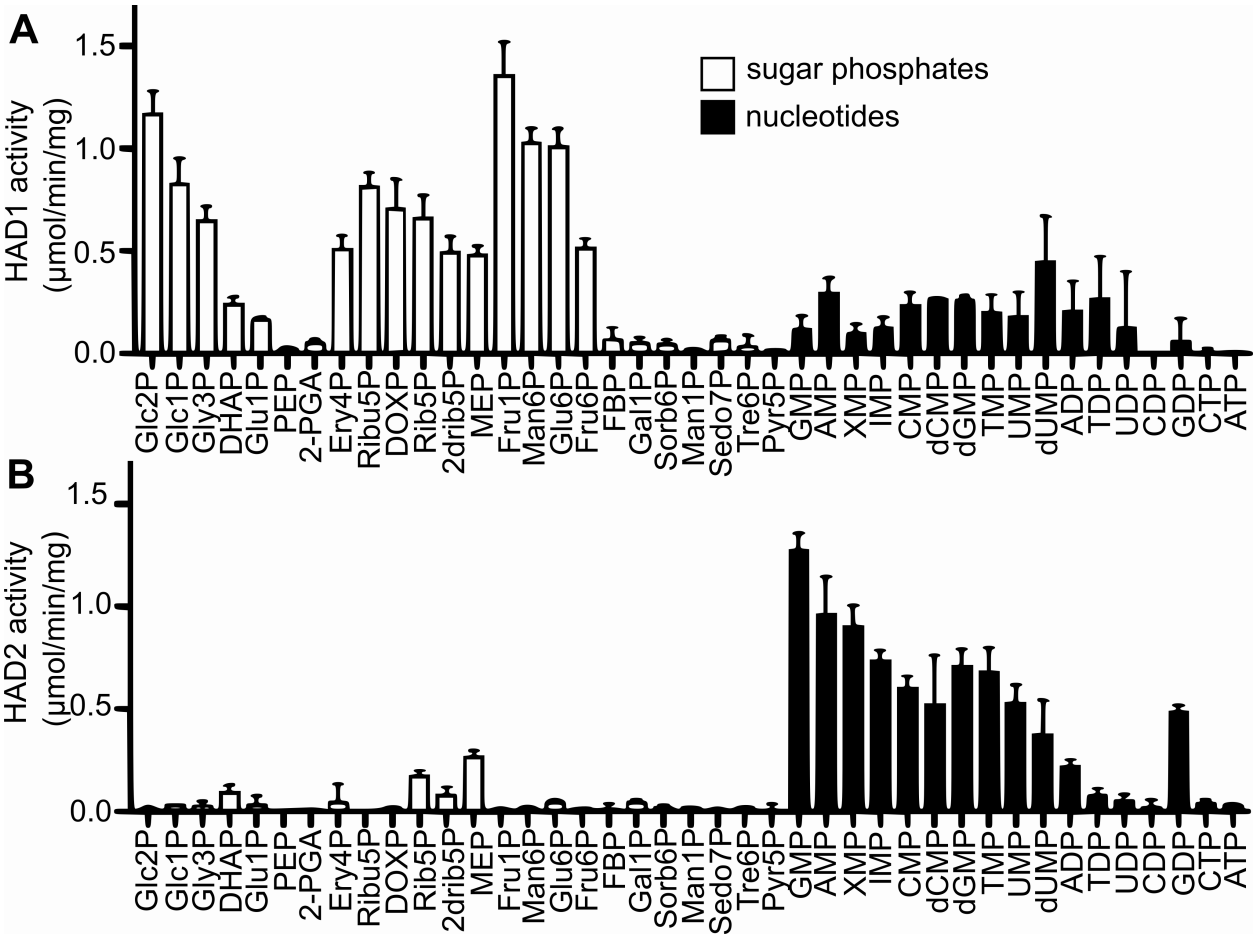

Figure 2. HAD2 is a nucleotidase.

Shown are mean specific enzyme activities for (**A**) HAD1 and (**B**) HAD2. Error bars represent S.E.M. (n≥3). HAD1 activity against sugar phosphates was previously described (Guggisberg, Park, et al., 2014). Sugar phosphates (white bars) are ordered from left to right by increasing number of carbon atoms (3-15). Nucleotides (black bars) are ordered from left to right by increasing degree of phosphorylation. Abbreviations: Glc2P, glycerol 2-phosphate; Glc1P, glycerol 1-phosphate; Gly3P, glyceraldehyde 3-phosphate; DHAP, dihydroxyacetone phosphate; Glu1P, glucose 1-phosphate; PEP, phosphoenolpyruvate; 2-PGA, 2-phosphoglyceric acid; Ery4P, erythrose 4-phosphate; Ribu5P, ribulose 5-phosphate; DOXP, deoxyxylulose 5-phosphate; Rib5P, ribose 5-phosphate; 2drib5P, 2-deoxyribose 5-phosphate; MEP, methylerythritol phosphate;

779 Fru1P, fructose 1-phosphate; Man6P, mannose 6-phosphate; Glu6P, glucose 6-phoshpate; Fru6P,
780 fructose 6-phosphate; FBP, fructose 1,6-bisphosphate; Gal1P, galactose 1-phosphate; Sorb6P,
781 sorbitol 6-phosphate; Man1P, mannose 1-phosphate; Sedo7P, sedoheptulose 7-phosphate; Tre6P,
782 trehalose 6-phosphate; Pyr5P, pyridoxal 5'-monophosphate; GMP, guanosine 5'-
783 monophosphate; AMP, adenosine 5'-monophosphate; XMP, xanthosine 5'-monophosphate; IMP,
784 inosine 5'-monophosphate; CMP, cytidine 5'-monophosphate; dCMP, 2'-deoxycytidine 5'-
785 monophosphate; dGMP, 2'-deoxyguanosine 5'-monophosphate; TMP, thymidine 5'-
786 monophosphate; UMP, uridine 5'-monophosphate; dUMP 2'-deoxyuridine 5'-monophosphate;
787 ADP, adenosine 5'-diphosphate; TDP, thymidine 5'-diphosphate; UDP, uridine 5'-diphosphate;
788 CDP, cytidine 5'-diphosphate; GDP, guanosine 5'-diphosphate; CTP, cytidine 5'-triphosphate;
789 ATP, adenosine 5'-triphosphate.
790

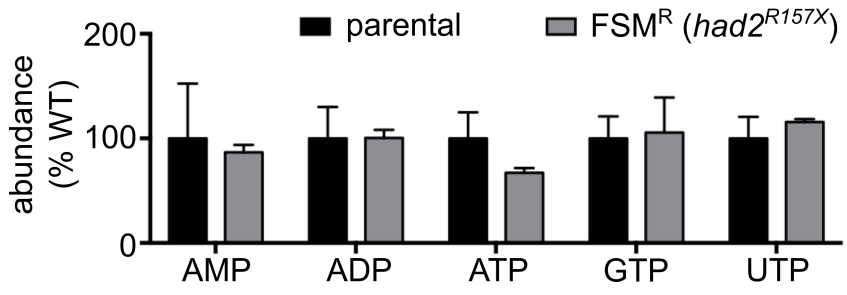

Figure 2-figure supplement 1. Nucleotide levels are unchanged in E2 FSM^R parasites.

Error bars represent S.E.M. (n=3). A full panel of nucleotides was assessed. Of those detected, no metabolite is significantly changed in the FSM^R (*had2*^{R157X}) strain ($p>0.05$, unpaired Student's t-test). Other nucleotides were below the limit of detection.

798

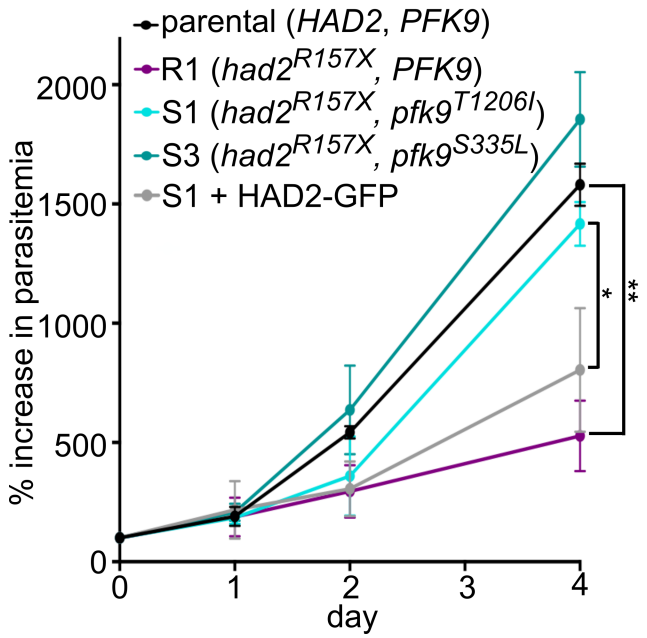

799

800 **Figure 3. FSM resistance results in a fitness cost.**

801 A representative FSM^{R} clone with the *had2*^{R157X} allele (R1, purple line) has a reduced growth
802 rate compared to the wild-type parental strain (black). The growth defect is rescued in two
803 representative clones with mutations in *PFK9* (S1 and S3, teal lines). Growth is normalized to
804 percent infected red blood cells on day 0. Error bars represent S.E.M. from independent growth
805 experiments ($n \geq 4$, ** = $p \leq 0.01$, * = $p \leq 0.05$, one-way ANOVA).

806

807

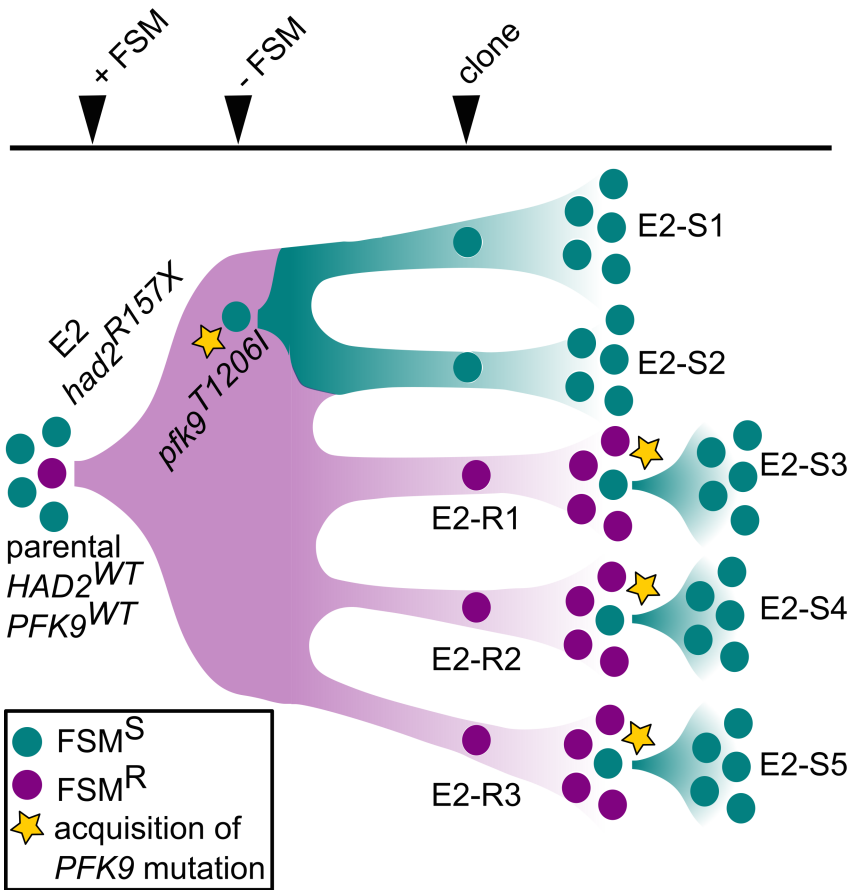

808

809 **Figure 4. Parasite selection scheme and genetic changes that modulate FSM sensitivity.**

810 Parasites are colored by their FSM phenotype (teal, FSM^S; purple, FSM^R). Cloned strains are

811 named by FSM phenotype (E2-SX, sensitive; E2-RX, resistant). A FSM^S parental strain was

812 selected under FSM pressure to enrich for FSM^R strain E2 (*had2*^{R157X}). After relief of FSM

813 pressure, a fitness advantage selects for spontaneous suppressor mutations in *PFK9* (*pfk9*^{mut},

814 yellow star) that result in FSM sensitivity. FSM^R clones are grown without FSM pressure and a

815 fitness advantage again selects for suppressor mutations in *PFK9* that result in increased growth

816 rate and loss of FSM resistance.

817

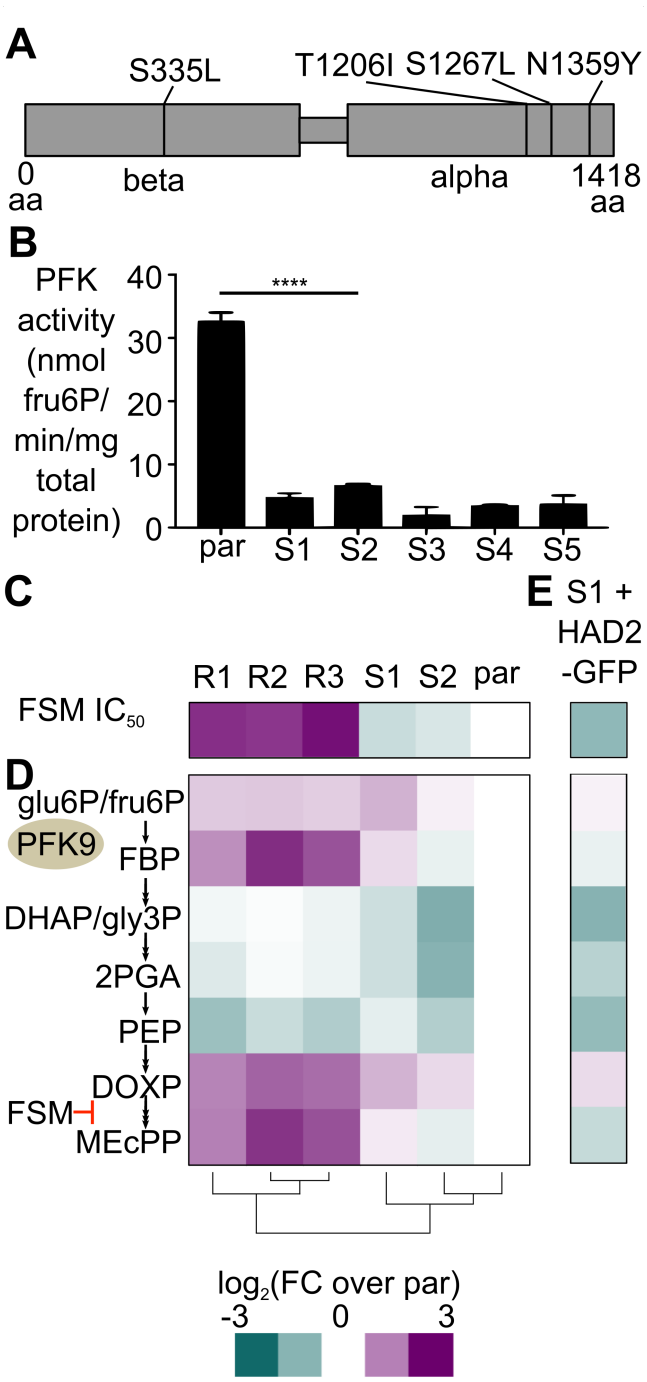

Figure 5. *HAD2* and *PFK9* alleles alter FSM resistance, PFK activity, and metabolite levels in *P. falciparum*.

For heatmaps, colors represent the $\log_2$ of the fold change (FC) over the parental strain, as indicated in the legend. Cloned strains are named by FSM phenotype (SX, sensitive; RX,

resistant). (**A**) Schematic of suppressor mutations identified in PFK9. Amino acid changes are shown. (**B**) Measurement of PFK activity of *P. falciparum* lysate indicates that E2-SX clones with *PFK9* suppressor mutations have significantly reduced PFK activity ($n \geq 3$, **** = $p \leq 0.0001$, one-way ANOVA). Error bars represent S.E.M. Assay is linear and specific for PFK activity (Figure 5-figure supplement 1). (**C**) FSM IC_{50}s for parental (par) strain and E2 clones. (**D**) Metabolic profiling and clustering of parental and E2 clone strains demonstrates a metabolic signature of resistance, which includes increased levels of MEP pathway intermediates DOXP and MEcPP and the glycolytic metabolite FBP. Data are representative of at least three independent experiments. Glu6P/fru6P and DHAP/gly3P represent isomer pairs that cannot be confidently distinguished. Clustering performed using the heatmap function in R. (**E**) When loss of HAD2 is rescued in $had2^{R157X}$, $pfk9^{T1206I}$ parasites, the resulting strain is hyper-sensitive to FSM, due to functional HAD2 and a hypomorphic *PFK9* allele.

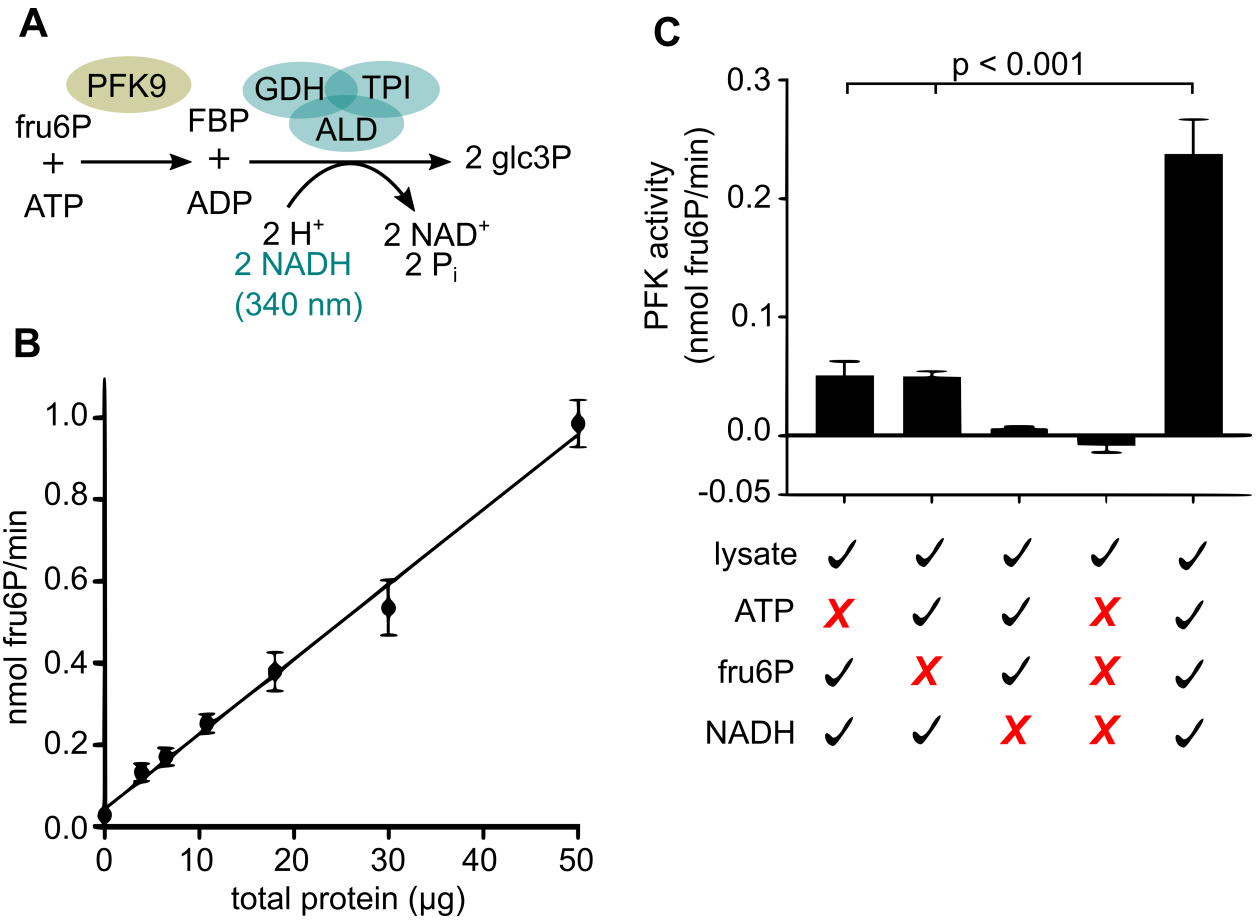

Figure 5-figure supplement 1. Assay of PFK activity from *P. falciparum* lysate is linear and specific.

(**A**) Schematic of linked enzyme assay of PFK activity. PFK catalyzes the phosphorylation of fructose 6-phosphate (fru6P) to fructose 1,6-bisphosphate (FBP). Excess linking enzymes aldolase (ALD), triose-phosphate isomerase (TPI), and glycerol 3-phosphate dehydrogenase (GDH) produce glycerol 3-phosphate. NADH utilization is monitored spectrophotometrically at 340 nm. (**B**) The assay is linear with respect to total lysate protein content. Error bars represent S.E.M. (n=2). (**C**) The assay is specific for *P. falciparum* lysate-dependent PFK activity and detects PFK activity above background (n=2, p<0.001). Error bars represent S.E.M.

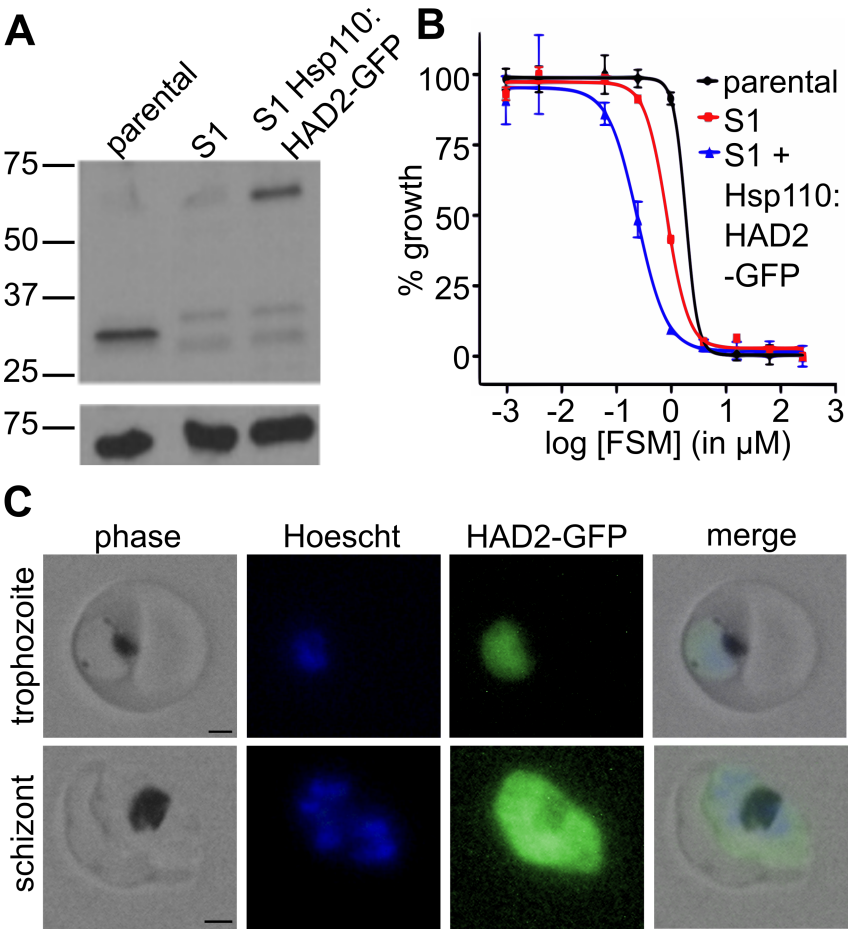

Figure 5-figure supplement 2. Rescue of HAD2 confirms its role as a negative regulator.

(**A**) Successful expression of pTEOE110:HAD2-GFP in strain S1 (*had2*^{R157X}, *pfk9*^{T1206I}) was confirmed by immunoblot. Marker units are kilodaltons (kDa). Expected sizes: HAD2, 33 kDa; HAD2-GFP, 60 kDa. The top blot was probed with anti-HAD2 antisera. The bottom blot was probed with anti-heat shock protein 70 antisera as a loading control. Blot is representative of three independent experiments. Minimal brightness adjustments were applied equally to all blot images. (**B**) Representative FSM dose-response demonstrating expression of HAD2-GFP in strain S1 (*had2*^{R157X}, *pfk9*^{T1206I}) results in oversensitivity to FSM. The parental strain has a FSM IC_{50} of 0.8 ± 0.1 µM, and S1 has an IC_{50} of 0.5 ± 0.08 µM. When loss of HAD2 is rescued in strain S1, the resulting strain has an IC_{50} of 0.3 ± 0.1 µM. Data shown are means and S.E.M. (n≥ 3). (**C**) Live microscopy of E2 HAD2-GFP parasites indicates that HAD2-GFP localizes to the

parasite cytoplasm. Hoescht 33258 was used as a nuclear stain. Scale bars, 2 μm. Image adjustments were applied equally to all images.

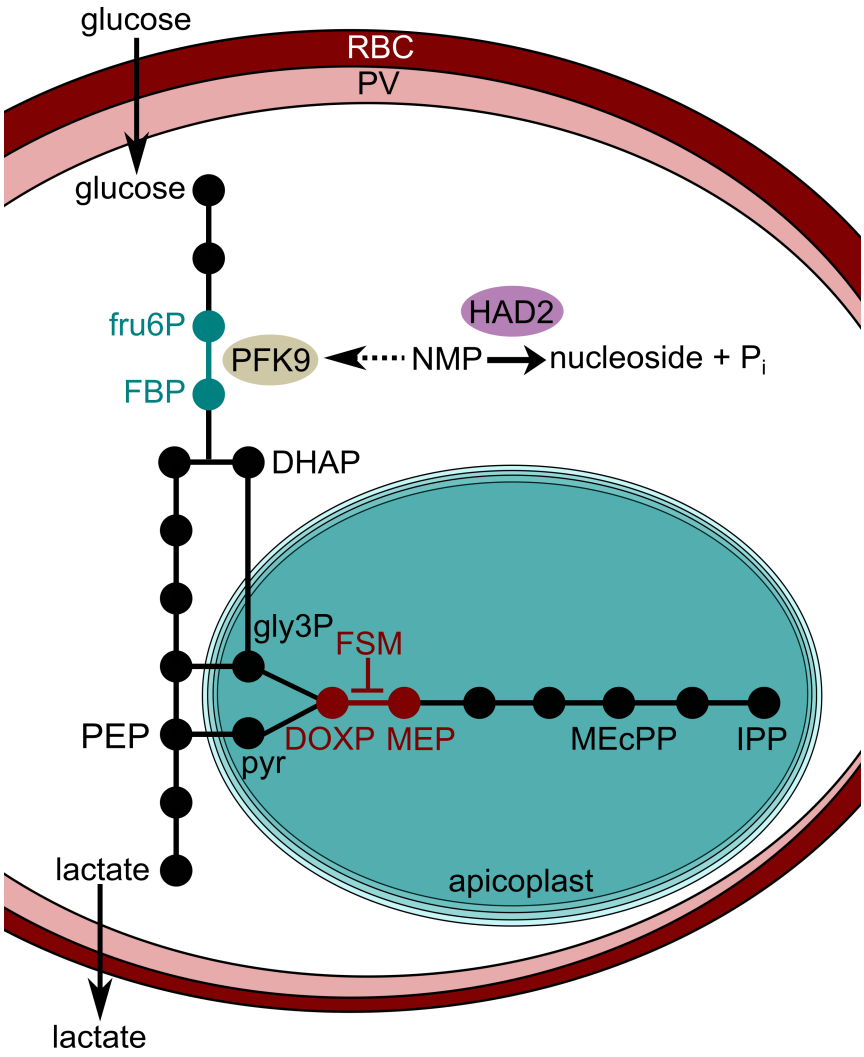

Figure 6. Model of HAD2-PFK9 metabolic regulation.

HAD2 may function as a negative glycolytic regulator at PFK9 by dephosphorylating nucleotides that function as positive allosteric regulators of PFK9. Loss of HAD2 results in increased flux through glycolysis and the MEP pathway, resulting in FSM resistance. Reduced PFK activity relieves this increased flux and restores FSM sensitivity. Abbreviations: RBC, red blood cell; PV, parasitophorous vacuole; NMP, nucleotide monophosphate.

874 **Table 1. Kinetic parameters for HAD2.**

875 Shown are the mean kinetic parameters for HAD2 against various substrates. Error bars represent
876 S.E.M. (n≥ 3). Abbreviations used: AMP, adenosine 5'-monophosphate; GMP, guanosine 5'-
877 monophosphate; 2dGMP, 2'-deoxyguanosine 5'-monophosphate; XMP, xanthosine 5'-
878 monophosphate; IMP, inosine 5'-monophosphate.

879

Substrate	K_m (mM)	K_{cat} (sec^{-1})	k_{cat}/K_m (M^{-1} sec^{-1})
AMP	1.0 ± 0.2	1.7 ± 0.3	1.7 x 10^3
GMP	0.30 ± 0.07	2.0 ± 0.1	6.9 x 10^3
2dGMP	0.30 ± 0.01	3.2 ± 0.5	11.0 x 10^3
XMP	0.73 ± 0.09	3.6 ± 0.1	5.0 x 10^3
IMP	8.4 ± 0.6	2.5 ± 0.1	0.30 x 10^3

880